International Journal of Heat and Mass Transfer 171 (2021) 121074

Contents lists available at ScienceDirect

International Journal of Heat and Mass Transfer

journal homepage: www.elsevier.com/locate/hmt

Numerical simulation of ultrasonic enhancement by acoustic streaming and thermal effect on mass transfer through a new computation model

Xingshuo Chen[a,b], Bayanheshig[a], Qingbin Jiao[a,*], Xin Tan[a], Wei Wang[a]

[a] Changchun Institute of Optics, Fine Mechanics and Physics, Chinese Academy of Sciences, Changchun 130033, China
[b] University of Chinese Academy of Sciences, Beijing 100049, China

ARTICLE INFO

Article history:
Received 17 September 2020
Revised 4 January 2021
Accepted 6 February 2021
Available online 19 February 2021

Keywords:
Mass transfer coefficient
Acoustic streaming
Thermal effect
Numerical simulation

ABSTRACT

Mass transfer coefficient is an important parameter in the process of mass transfer to reflect the degree of enhancement of mass transfer process in liquid–solid reaction and in non-reactive systems. In the present paper, a new computational model including both acoustic streaming and ultrasonic thermal effect is established to quantitatively calculate the ultrasonic enhancement on mass transfer coefficient in liquid–solid reaction. A nonlinear Helmholtz equation containing the cavitation effect is used in the model to calculate the acoustic pressure distribution in the reactor, and a fluid-thermal coupling CFD involving mass transfer process for KOH solution is conducted to obtain the distribution and time-dependence of the mass transfer coefficient in silicon–KOH reaction. Mass transfer coefficient on silicon surface with a transducer at frequencies of 100 kHz has been numerically simulated, indicating that the mass transfer coefficient has the maximum value near the center of the silicon wafer, and increases with reaction time. The mass transfer coefficient in the center of the silicon wafer is increased by 14.3% from 6.043×10^{-5} m/s to 6.908×10^{-5} m/s under ultrasound power of 50W during reaction time from 0.1 hour to 1 hour (the mass transfer coefficient without ultrasound changes from 2.525×10^{-6} m/s to 7.615×10^{-7} m/s). A set of control simulations shows that the enhancement of mass transfer coefficient comparing to the situation without ultrasound is mainly resulted from the acoustic streaming, while the increasing of mass transfer coefficient with time is due to the thermal effect of ultrasound. The mass transfer coefficients under transducer power of 10W and 30W are also calculated, indicating that the mass transfer coefficient is positively correlated with the ultrasonic power.

1. Introduction

The intervention of ultrasound has been widely applied in liquid-solid reactions to improve the reaction rate and enhance the mass transfer process [1–4]. As an important parameter to describe mass transfer, mass transfer coefficient can quantitatively reflect the degree of enhancement on mass transfer process in liquid-solid reaction and in non-reactive systems [5–10], which is important for the selection of ultrasonic parameters and the structural optimization of the ultrasonic reactor. Thus, it is an important thing to study the effect of ultrasound on the mass transfer coefficient quantitatively.

The enhancement of mass transfer by ultrasonic is mainly a result of cavitation effect. The instantaneous high temperature and high pressure caused by cavitation bubble collapse will accelerate the reaction rate. Meanwhile, the strong attenuation caused by cavitation will produce significant acoustic streaming [11–14] and thermal effect [15–17]. However, conventional cavitation theory such as electrical theory [18–20] and hot spot theory [21,22] mainly focus on the study of a single cavitation bubble, making it difficult to quantitatively describe the effect of cavitation on the whole mass transfer process. In recent years, O. Louisnard [23–26] proposed a sound field propagation theory considering cavitation effect by associating the bubble dynamic equation with the sound attenuation coefficient in the Helmholtz equation, which was further improved by R. Jamshidi [27] and F. J. Trujillo [28,29] *et al.* This theory makes it possible to construct multi-physical field simulation containing cavitation effect.

* Corresponding author.
E-mail address: jqbyyawyx@163.com (Q. Jiao).

https://doi.org/10.1016/j.ijheatmasstransfer.2021.121074
0017-9310/

The acoustic streaming and thermal effect caused by ultrasound have great influence on the mass transfer process. Acoustic streaming in the reactor will enhance the heat transfer process, change the concentration distribution of solution, and facilitate the process of mass exchange. Meanwhile, the ultrasonic thermal effect will increase the temperature of the solution, thus affecting the thermophysical properties of the solution and the reaction rate, which will further enhance the acoustic streaming and the mass transfer process. Therefore, the acoustic streaming and the thermal effect caused by ultrasound are mutually coupled, and both affect the mass transfer process.

However, theoretical studies on the effect of ultrasound on mass transfer are rare due to the complexity of the physical mechanism. Jiao *et al.* [30] put forward a computational model to quantitatively calculate the mass transfer coefficient of KOH-silicon surface through numerical simulation. Nevertheless, the above model did not consider the thermal effect and heat transfer process caused by ultrasound, and an empirical constant 5 m^{-1} was used as the sound attenuation coefficient, which reduced the accuracy of the theoretical model. Moreover, the fluid-thermal coupling CFD simulation for KOH electrolyte solution has not been reported in existing literature.

In the present paper, a new multi-physical field model is developed to quantitatively describe the enhancement of mass transfer by ultrasound, which includes both acoustic streaming and the thermal effect. The interaction of the flow field, the temperature field and the mass transport field in KOH solution is considered in the theoretical model. The numerical simulation is carried out in two parts: i) A nonlinear Helmholtz equation containing the cavitation effect is used to calculate the acoustic pressure distribution in the reactor, which further gives the distribution of volume force and heat source; ii) Fluid-thermal coupling CFD involving mass transfer process is conducted to obtain the transient behavior of major physical quantities in the model. The time-dependence of mass transfer coefficient and its relationship with acoustic streaming and thermal effect are emphatically analyzed. The effect of ultrasonic power on mass transfer coefficient is also discussed in our manuscript.

2. Computational model

2.1. Acoustic pressure field

Considering the energy loss of ultrasound caused by cavitation effect, the acoustic field in the reactor can be ascribed as a nonlinear inhomogeneous Helmholtz equation [24]:

$$\nabla^2 P - k_c^2 P = 0 \tag{1}$$

in which P represents the acoustic pressure. The complex acoustic wave vector k_c is related to the sound attenuation coefficient α:

$$k_c = k_r - i\alpha \tag{2}$$

$$c_c = \frac{\omega}{k_c} \tag{3}$$

The angular frequency ω is defined by the ultrasound frequency f as ω=2πf, while c_c represent the speed of sound in the media.

Due to the direct dependence of volume force and heat source on the sound attenuation coefficient α, it is necessary to select a reasonable value of the attenuation coefficient. According to O. Louisnard's theory [23–26], the attenuation coefficient is related to the amplitude of the sound pressure, and mutates near the Blake threshold. The method of R. Jamshidi [27] is used in this paper to calculate the attenuation coefficient α, in which the Keller-Miksis Equation is applied on the radical dynamics of cavitation bubbles [31,32]:

$$\rho\left(\left(1-\frac{\dot{R}}{c}\right)R\ddot{R}+\frac{3}{2}\dot{R}^2\left(1-\frac{\dot{R}}{3c}\right)\right) = \left(1+\frac{\dot{R}}{c}+\frac{R}{c}\frac{d}{dt}\right)\left(p_g-\frac{2\sigma}{R}-\frac{4\mu\dot{R}}{R}-p\right) \tag{4}$$

R and p_g respectively represent the initial radius of a single bubble and the pressure inside the bubble. p represents the external pressure, which can be expressed as $p = P_0$ - Psin(ωt), where P_0 is the environmental pressure. Considering the effect of heat transfer at the boundary layer, the pressure inside the bubble satisfies the ODE as below:

$$\dot{p}_g = p_g\gamma\left(\frac{-3\dot{R}}{R}\right)+(\gamma-1)\left(k\frac{3}{R}\frac{dT}{dr}\right) \tag{5}$$

where k represents the conductivity of the gas, T represents the temperature inside the cavitation bubble. The temperature gradient dT/dr at the bubble surface can be approximated as:

$$\frac{dT}{dr} = \frac{T-T_\infty}{\delta} \tag{6}$$

in which δ is the thermal boundary thickness:

$$\delta = \sqrt{\frac{R\kappa}{3(\gamma-1)\dot{R}}} \tag{7}$$

κ represents the thermal diffusivity of the gas. The temperature in the cavitation bubble follows the first law of thermodynamics:

$$C_v\dot{T} = \dot{Q} - p\dot{V} \tag{8}$$

The constant volume heat capacity $C_v = 5/2nk_B$, n represents the number of gas molecules in the bubble. More detailed process can be referred to Ref. [33].The energy loss of sound field caused by a single cavitation bubble can be expressed as:

$$\Pi_{th} = \frac{1}{T}\int_0^T -\left(p_g\left(1+\frac{\dot{R}}{c}\right)+\frac{R}{c}\frac{dp_g}{dt}\right)\frac{\partial V}{dt}dt \tag{9}$$

$$\Pi_v = \frac{1}{T}\int_0^T 16\pi\mu\left(R\dot{R}^2+\frac{R^2\dot{R}\ddot{R}}{c}\right)dt \tag{10}$$

$$\Pi_r = \frac{4\pi}{Tc}\int_0^T R^2\dot{R}\left(\dot{R}p+\dot{p}R-\frac{1}{2}\rho\dot{R}^3-\rho R\dot{R}\ddot{R}\right)dt \tag{11}$$

The T here refers to the period of the sound wave. The above three items represent the acoustic field energy loss caused by heat conduction, viscosity and acoustic radiation force, respectively. The square of the wave number satisfies the following relation:

$$\Im\left(k_c^2\right) = -2\rho wN\frac{\Pi_{th}+\Pi_v+\Pi_r}{|P|^2} \tag{12}$$

$$\Re\left(k_c^2\right) = \frac{\omega^2}{c^2}+\frac{4\pi R_0\omega^2 N}{\omega_0^2-\omega^2} \tag{13}$$

in which N represents the bubble density of the liquid, ω_0 represents the resonant frequency of the bubble, which can be calculated by following equations:

$$\chi = \frac{\alpha_t}{\omega R_0^2} \tag{14}$$

$$\Phi = \frac{3\gamma}{1-3(\gamma-1)i\chi\left[(i/\chi)^{1/2}\coth(i/\chi)^{1/2}-1\right]} \tag{15}$$

$$\omega_0^2 = \frac{p_0}{\rho R_0^2}\left[\Re(\Phi)-\frac{2\sigma}{p_0R_0}\right] \tag{16}$$

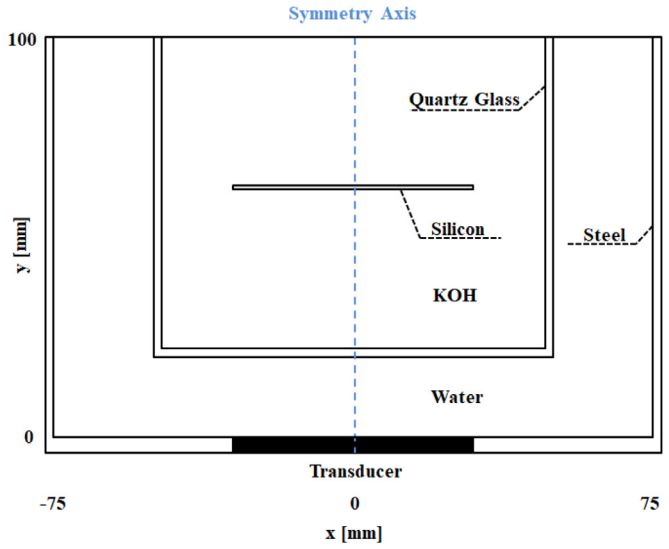

Fig. 1. The schematic diagram of reactor geometric structure.

According to Eq (12) and Eq (13), the wavenumber k_c can now be expressed as the form of Eq (2), which is composed of the real part of the wave number and the attenuation coefficient:

$$k_c = k_r - i\alpha \tag{17}$$

The ultrasound frequency used in the simulation is 100 kHz. The initial radius of the cavitation bubble is set at 5 μm and the bubble density N is set to a constant of $5^{*}10^{9}/m^{3}$ for the calculation of the attenuation coefficient, which has been verified by Louisnard [24,25] and Trujillo [27] that this setting conformed well to the experimental results. Since the energy loss caused by liquid viscosity is not the main part of attenuation, the difference of attenuation coaefficient between KOH solution and water is ignored in the calculation. Bubble dynamic equations from Eq (4) to Eq (8) are solved by using variable order numerical differential algorithm (ODE15S) in MATLAB. It is worth mentioning that the Jamshidi's model used above contains some approximations, including the representation of thermal boundary conditions and the omissions of water evaporation and condensation processes. Some more sophisticated theories, such as the thermal boundary layer model described by Preston [34] and Zhang [35], and the bubble dynamics model including phase transitions used by Caflisch [36] and Bergamasco [37], can be further applied to the solution of bubble dynamics and the calculation of sound attenuation coefficient for further improvement of the model.

The sound field was calculated in a reactor model with a width of 150mm and a height of 100mm, and the symmetric condition is applied to the model, as shown in Fig. 1. The model is divided into two fluid regions by a quartz glass container with 2mm in thickness: the inner layer is KOH solution with a concentration of 10wt%, while the outer layer is water. A piece of silicon wafer with 30 mm in radius and 1 mm in thickness was placed in the center of the container. An ultrasound transducer with a radius of 30mm was placed at the bottom of the reactor, which was set as the acoustic pressure boundary. Since the outer wall of the reactor is made of steel, the outer boundary was set as the boundary of hard sound field to simplify the calculation. The quartz-air and the liquid-air interface at the top of the reactor, as well as the liquid-quartz interface inside the reactor were subject to impedance boundary conditions. The density and sound velocity of medium is shown in Table 1 [38].

Table 1
The density and sound velocity of medium [34].

Medium	Density (kg/m^3)	Sound velocity (m/s)
Water	1000	1500
Quartz glass	2700	5760
Monocrystalline silicon	2330	7140
KOH solution (10%)	1054	1500

2.2. The flow field

The flow field can be calculated by the momentum transport equation:

$$\rho\left(\frac{\partial \vec{v}}{\partial t} + \vec{v}\cdot\nabla\vec{v}\right) = -\nabla p + \mu\nabla^2\vec{v} + \vec{F} \tag{18}$$

where $\boldsymbol{v}$ represents the velocity of fluid motion, p is the sound pressure, and F represents the volume force. The acoustic streaming in the container can be described by the time averaged version of the Navier–Stokes equation, which contains the inertia term modified by Lighthill [39]:

$$\rho(\bar{v}\cdot\nabla\bar{v}) = -\nabla p + \mu\nabla^2\bar{v} + \vec{F} \tag{19}$$

in which $\boldsymbol{F}$ represents the volume force that causes the acoustic streaming:

$$\left\langle\vec{F}\right\rangle = -\rho_0\langle(\vec{v}_{ac}\cdot\nabla)\vec{v}_{ac} + \vec{v}_{ac}\nabla\cdot\vec{v}_{ac}\rangle$$

$\boldsymbol{v}_{\mathrm{ac}}$ represents the oscillating velocity of the medium. A plane wave approximation is used since the acoustic wavelength is much smaller than the scale of the reactor, and the volume force is expressed by Eq. 20 [13,40]:

$$F = \frac{2\alpha I}{c} \tag{20}$$

where I stands for sound intensity. The no slip wall is used as the boundary condition of the flow field area, except the interface between fluid and air. Considering the temperature rise effect caused by ultrasound, the viscosity of 10wt% KOH solution can be calculated by an empirical formula obtained by Guo *et al.* [41,42], in which T_c represents the value of temperature in terms of Celsius degree:

$$\mu_{KOH} = 10^{-3}\exp\left(0.43 - 0.0251T_c + 10^{-4}T_c^2 + 0.246\right)Pa\cdot s \tag{21}$$

According to Lighthill's theory [39], the acoustic streaming caused by ultrasound is mostly a turbulent jet dominated by inertia. Therefore, the k-ω turbulence model was first used to calculate the two fluid regions in the reactor. The result showed that the flow field in the outer water region had obvious turbulence characteristics, and the maximum turbulence kinetic energy was in the magnitude of $10^{-4}m^2/s^2$. Nevertheless, the turbulence variable of internal KOH solution is almost zero and can be ignored. This result can be explained by the reflection of sound waves by the silicon dioxide layer in the reactor and the significant difference in the sound attenuation coefficient between the inner and outer regions. Therefore, we finally use the laminar flow model and the k-ω turbulence model to calculate the internal and external flow field, respectively.

2.3. The temperature field

The temperature change in the reactor can be expressed by the energy conservation equation:

$$\rho C_p\left(\frac{\partial T}{\partial t} + v_x\frac{\partial T}{\partial x} + v_y\frac{\partial T}{\partial y}\right) = k_{eff}\left(\frac{\partial^2 T}{\partial x^2} + \frac{\partial^2 T}{\partial y^2}\right) + Q \tag{22}$$

where ρ,C_p are the density and the constant pressure heat capacity of material, k_{eff} represents the effective heat transfer coefficient,

v_x,v_y are the velocity components of the fluid field. The heat source Q is provided by the dissipation of the sound field in the fluid, which can be expressed as [43,44]:

$$Q = 2\alpha I \tag{23}$$

Eq (23) contains a plane wave approximation to simplify the calculation process. According to the calorimetric method for measurement of acoustic power [45], the dissipated energy for heat generation could be equal to the energy emitted by the source if the acoustic energy is absorbed close to the source. However, this assumption is not suitable for our model, for the attenuation coefficient decreases rapidly with the reducing of sound pressure, resulting in the difference between the dissipated energy and the total acoustic energy. The heat capacity C_p of KOH solution is derived from Ref. [42].

For solid materials in the reactor, the convection term and the heat source term are zero, and the energy equation is:

$$\rho C_p \frac{\partial T}{\partial t} = k_0 \nabla^2 T \tag{24}$$

The interface between the internal solid and fluid is coupled by the continuity condition of heat flux and temperature. The external boundary conditions of the model are described as the convective heat transfer process between the reactor wall and the external air, as well as between the fluid surface and the external air. The external environmental temperature T_{ext} is 20°C. The heat transfer process follows Newton's cooling law by setting the convective heat transfer coefficient h:

$$-\vec{n} \cdot (-k_0 \nabla T) = h(T_{ext} - T) \tag{25}$$

In the outer turbulent field of the reactor, The enhanced effect of turbulence on heat exchange is described by the effective heat transfer coefficient k_{eff} [17]:

$$k_{eff} = k_0 + \frac{C_p \mu_t}{\mathrm{Pr}} \tag{26}$$

in which k_0=0.6W/m^{2}K is the original heat transfer coefficient of water, μ_t represents the turbulent dynamic viscosity of the external flow field, and Pr is the Prandtl number of water. Distribution of the effective heat transfer coefficients is updated with iterations according to the transient results of the turbulence model. The heat transfer coefficient of 10wt% KOH solution could be expressed as [42]:

$$k_{KOH} = 5.545 \cdot 10^{-1} + 2.460 \cdot 10^{-3} T_c - 1.169 \cdot 10^{-5} T_c^2 W \cdot m^{-1} K^{-1} \tag{27}$$

2.4. The mass transport field

Mass transfer in KOH solution is calculated by the mass transfer differential equation:

$$\frac{\partial c}{\partial t} + \nabla \cdot (-D \nabla c) + \vec{u} \cdot \nabla c = 0 \tag{28}$$

where c, D and u respectively represent the solution concentration, the mutual diffusion coefficient and the velocity distribution. Considering the influence of temperature rise effect on solute diffusion, the mean spherical approximation (MSA) method [46] and the Nernst-Einstein equation [47] are used to calculate the change of mutual diffusion coefficient D of 10wt% KOH solution with Kelvin temperature T. The result is fitted as a linear function and substituted into the mass transfer equation for calculation:

$$D = 10^{-10}(0.096 \cdot T - 1.980) m^2 s^{-1} \tag{29}$$

For the reaction interface between silicon and KOH solution, the boundary conditions are as follows:

$$-\vec{n} \cdot N_c = q \tag{30}$$

where N_c is the mass flux on silicon surface, q is the surface reaction rate whose unit is mol/m^2 s. For KOH solution with the concentration of 10wt%, The reaction between silicon and KOH solution can be seen as a 1/4 order irreversible reaction, and the reaction rate satisfies the Arrhenius equation [48]:

$$q = k_0 \exp(-E_a/RT) c_{AS}^{0.25} \tag{31}$$

in which E_a represents the apparent activation energy, c_{AS} is surface concentration of KOH solution, k_0 is the rate constant with unit of mol$^{0.75}$/(m$^{1.25}$s), and R is the molar gas constant. The apparent activation energy and the rate constant under ultrasound of 100 kHz have been measured in our previous work by Jiao *et al* [49].

According to Eq (31), the boundary flux in the simulation is a function of the surface temperature T and the surface concentration c_{AS}, where the temperature T is provided by the temperature field, and the surface concentration is substituted into the calculation as an unknown quantity to be solved. The initial concentration of KOH solution used in the simulation was 1882mol/m^3. The mass transfer coefficient of the reaction interface is calculated by using Eq (32) [50], where c_A is the main molarity of KOH solution, N_c represents the mass flux at the boundary.

$$k_c = \frac{-N_c}{c_{AS} - c_A} \tag{32}$$

The above numerical model is constructed by the Finite Element Method in COMSOL Multiphysics™. The steady distribution of sound field in the reactor is firstly calculated to obtain the distribution of volume force and heat source. Then, the fluid field, temperature field and mass transfer field are calculated by coupling transient iteration. The mass transfer coefficient k_c of silicon-KOH reaction interface is eventually calculated according to the results of mass transfer field.

3. Results and discussion

3.1. Acoustic pressure distribution

Fig. 2 shows the dissipated energy and the wave number calculated under different sound pressures according to the above theory in Section 2.1, where the imaginary part of the wave number represents the value of sound attenuation coefficient. The parameters used in the calculation are shown in Table 1, where the bubble density is set as 5*10^9/m^3, as we discussed in Section 2.1. The obtained results have the same characteristics as the results of R. Jamshidi [27], showing that the heat transfer term and radiation term are much higher than the viscosity term under high sound pressure, and the radiation term is negative when the sound pressure is low.

Table 2

As shown in Fig. 2 (b), within the sound pressure range of 15-250 kPa, the sound attenuation coefficient ranges from 0.04-705 Np/m. As described by Louisnard [24] and Trujillo [29], when the imaginary part of the wave number is larger than the real part, the change of the real part of the wave number can be ignored and described linearly due to the dominant role of the sound attenuation coefficient. Fig. 3 shows the simulation result of acoustic pressure

Table 2
Physical properties set for the KM equation and wave number calculation.

R_0 (μm)	f (kHz)	k (W/m K)	κ (m^2/s)	γ	μ (Pa s)
5.0	100	2.60 e-2	2.19 e-5	1.4	1.0 e-3
P_0 (Pa)	C_v (J/K)	σ (N/m)	ρ (kg/m^3)	c (m/s)	N (1/m^3)
1.013 e5	5.86 e-13	7.5 e-2	1000	1500	5.0 e9

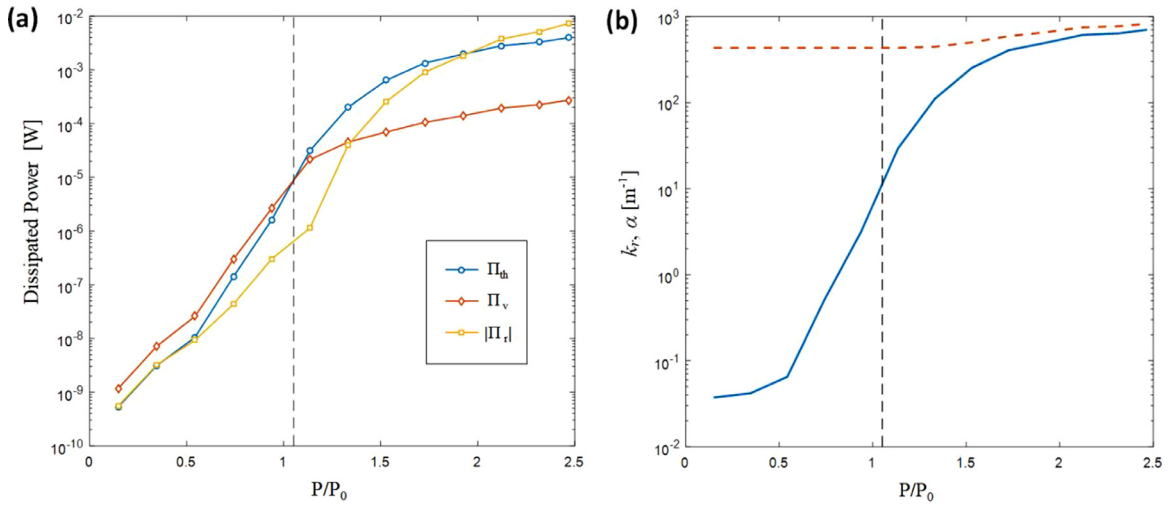

Fig. 2. (a) Acoustic power dissipated by a 5 μm air bubble at 100 kHz versus the normalized acoustic pressure amplitude. (b) Real part (red dash line) and imaginary part (blue solid line) of the wave number k. The vertical dash line represents the Blake threshold.

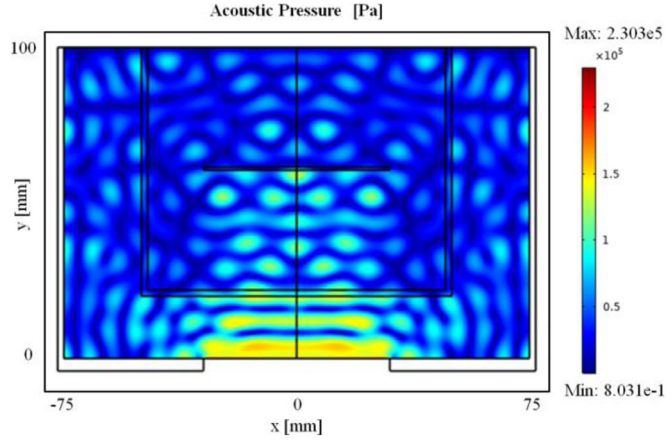

Fig. 3. Simulation of pressure field distribution with input power of 50 W.

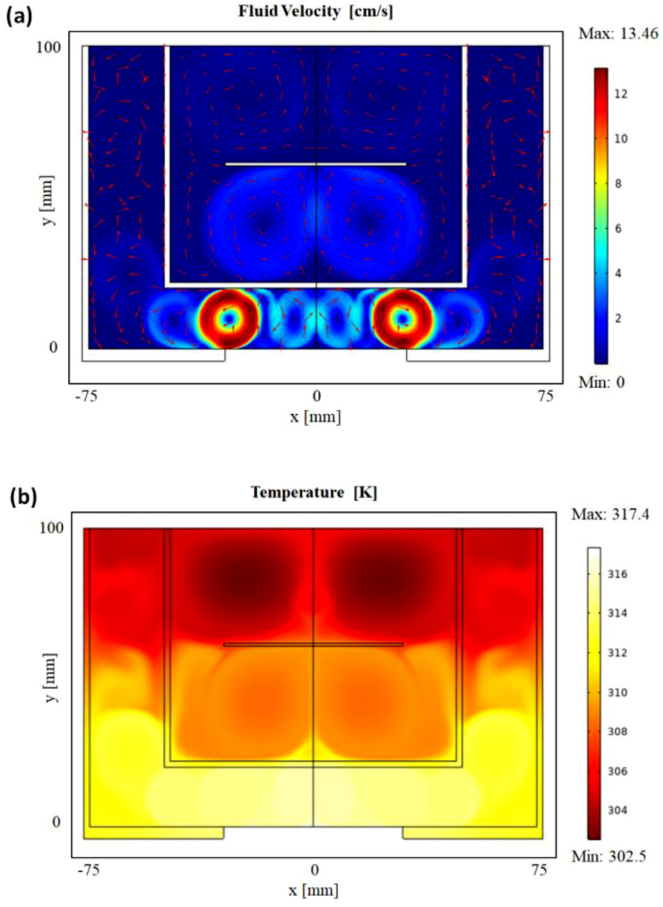

Fig. 4. (a) Velocity and (b) temperature distributions after one hour of ultrasonic treatment.

distribution in the reactor with input power of 50 W. The ordinate and abscissa in the figure represent the space position in reactor. Due to the positive correlation between sound attenuation coefficient and sound pressure, the high ultrasonic pressure can only be observed near the transducer surface, and attenuates rapidly in a short distance from the transducer. The pressure field was mainly concentrated in the transducer area (|x|<30mm) due to the high directivity of the ultrasound at 100 kHz.

3.2. Liquid velocity and temperature distribution

As described in the last part of Section 2, a fluid-thermal coupling CFD was used to calculate the transient distributions of the velocity and temperature fields. Fig. 4 shows the velocity distribution and temperature distribution in the reactor after one hour of ultrasonic treatment. The flow field was divided into two regions by the quartz container: due to the high sound pressure and sound attenuation coefficient, the area near the transducer has larger volume force, resulting in the obvious turbulence characteristics of the external flow field, and the maximum velocity is 13.5cm/s. Meanwhile, as the volume force of the internal solution is much smaller than that of the external flow field, the internal flow field is laminar, with a maximum velocity of 2.75cm/s. The k-ω turbulence model and laminar flow model for the internal flow have given the same result with no turbulence. Compared to simulations of Xu [13] and Jiao [30] with constant sound attenuation coefficients, the effect of sound pressure on the volume force is nonlinear and more significant, due to the positive correlation between the attenuation coefficient and sound pressure.

The temperature distribution of the reactor after one hour of ultrasonic treatment is shown in Fig. 4(b), and the maximum temperature of the reactor is 317.4K at t=1h. The power density at

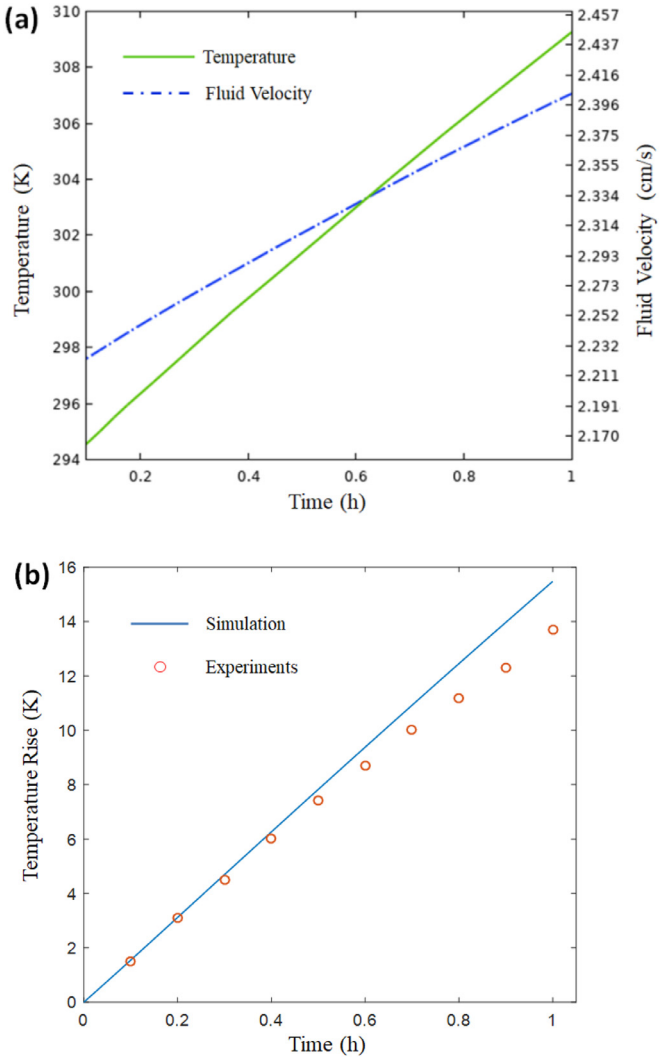

Fig. 5. (a) Temperature (green line) and the velocity (blue line) of the coordinate (0, 50) from 0.1h to 1h. (b) Theoretical and measured values of the average temperature rise of the reactor under ultrasound power of 50W.

each position for heat generation is proportional to the attenuation coefficient and the sound intensity, with an average power density of 19.6kW/m^3, which accounts for 67% of the total power of 50W. It can be clearly seen that the heat source derived from the acoustic energy loss is mainly concentrated near the transducer, which has the same characteristics as the volume force, and the convective heat transfer caused by acoustic streaming contributes greatly to the temperature distribution in the reactor. The enhancement of heat transfer by turbulence is taken into account by using the effective heat transfer coefficient k_{eff}, and the maximum value of k_{eff} in the outer region is 8.24W/(m•K) at t=1h, which is more than one order of magnitude higher than the original heat transfer coefficient of water.

3.2.2. Time dependence of velocity and temperature

Due to the combined effect of ultrasonic heat effect and acoustic streaming, the velocity and temperature distribution in the reactor is a transient rather than a steady state process. Fig. 5 (a) shows the changes of temperature and flow velocity at coordinates (0, 50) in the reactor with the ultrasonic processing time. As the temperature rises gradually under ultrasound, the viscosity of KOH solution decreases, leading to the gradual increase of the flow velocity, which further promotes the heat and mass transfer process. From 0.1h to 1h, the velocity of the coordinate (0, 50) rises 8.11% from 2.22cm/s to 2.40cm/s, while the highest velocity of the KOH solution increases by 11.0% from 2.49cm/s to 2.75cm/s. Thus, the comprehensive consideration of both thermal effect and acoustic stream effect of ultrasound is necessary for the simulation of mass transfer process.

We measured the values of average temperature rise in the reactor to briefly verify the rationality of the theoretical model, as shown in Fig. 5 (b). The experimental results are in good agreement with the theoretical values, with an error of 11.4% at t=1h, which might result from the structural difference between the model and the actual reactor. It also indicates the assumption that the power of heat generation is equal to the total acoustic power is not suitable for our model, as described in Section 2.3.

3.3. Mass transfer process

The mass transfer process is influenced by both the velocity field and the temperature field: the flow of the solution will promote the solute transfer and increase the concentration of the solution at the reaction interface, while the increase of temperature will significantly increase the rate of liquid-solid reaction, and lead to the increase of diffusion coefficient, promoting the mass transfer process. To describe the mass transfer process, we use several parameters including surface concentration c_{AS}, reaction rate q, and especially mass transfer coefficient k_c. Fig. 6 (a) shows the time dependence of the surface concentration c_{AS} on the lower surface of the silicon wafer from 0 to 1 hour. Due to the symmetry of the geometry, only the right side of the wafer is shown in the figure, and the zero of the X-axis represents the center of the silicon wafer. During the reaction, the surface concentration of silicon wafers continued to decline, mainly due to two reasons: the decrease of the total amount of solute in the reactor, and the rapid increase of reaction rate caused by temperature rise, as shown in Fig. 6 (b). In terms of space, the surface concentration distribution has a maximum value near the center of the silicon wafer, which is resulted from the distribution of fluid velocity and the convective mass transfer process. The uneven distribution of surface concentration plays a decisive role in the spatial characteristics of mass transfer coefficient, as shown in Fig. 7.

In order to ensure the accuracy of mass transfer coefficient calculation, the reasonable selection of the main concentration c_A is necessary. In this paper, we chose the concentration at coordinate (0, 45) with the highest flow velocity as the main concentration of c_A, where the mass exchange was the most sufficient and the concentration was uniform. Fig. 7 shows the simulation results of mass transfer coefficient under ultrasound with frequency at 100 kHz and ultrasound power of 50 W, from 0.1 h to 1.0 h. In terms of spatial distribution, the mass transfer coefficient k_c shows the similar characteristics of the surface concentration, which is caused by the inverse relation between the mass transfer coefficient and the concentration difference between c_{AS} and c_A, as shown in Eq (32). In terms of time, the mass transfer coefficient k_c shows a trend of continuous increase. k_c in the center of the silicon wafer have increased by 14.3% after 1 hour of ultrasound treatment compared with k_c at 0.1 hour, from 6.043e-5 m/s to 6.908e-5 m/s. This trend is due to the temperature rise effect caused by ultrasound, which will be discussed in detail in the next section.

3.3.1. Influence of acoustic streaming and thermal effect

A set of control simulations were carried out in order to further discuss the influence of ultrasonic acoustic streaming and thermal effect on mass transfer coefficient. Fig. 8 shows the changes of mass transfer coefficients with reaction time under three simulated conditions: considering both acoustic streaming and thermal

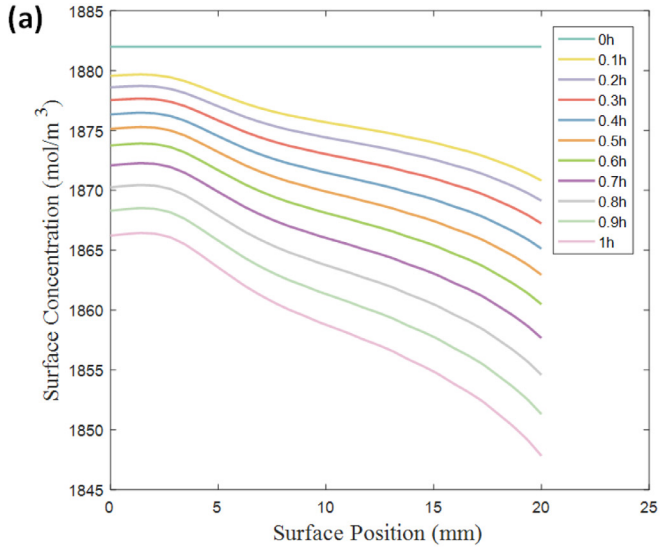

Fig. 6. (a) Surface concentration of the silicon wafer (Right side) from 0-1.0 h. The initial value of the concentration is 1882 mol/m^3. (b) The surface reaction rate of hydroxide ions from 0-1.0 h.

effect, considering acoustic streaming only, and no external ultrasound, respectively.

The mass transfer coefficients of different simulations show distinct characteristics: In the simulation without ultrasound, solute transfer can only be carried out through diffusion, and the transmission rate is lower than the consumption rate of the reaction interface, which leads to the increasing gap between the surface concentration and the main concentration and the continuous decrease of the mass transfer coefficient k_0 from 4.616e-6 m/s to 7.615e-7 m/s. When only acoustic streaming effect is considered, the mass transfer coefficient k_{as} has been greatly enhanced compared to k_0 and remains constant in the one-hour transient simulation, for the difference between c_{AS} and c_A decreases significantly under the acoustic streaming and remains stable during the reaction. And yet in the results obtained by the fluid-thermal coupling model, the mass transfer coefficient shows an obvious trend of increasing with time. Thus, it can be seen clearly from the com-

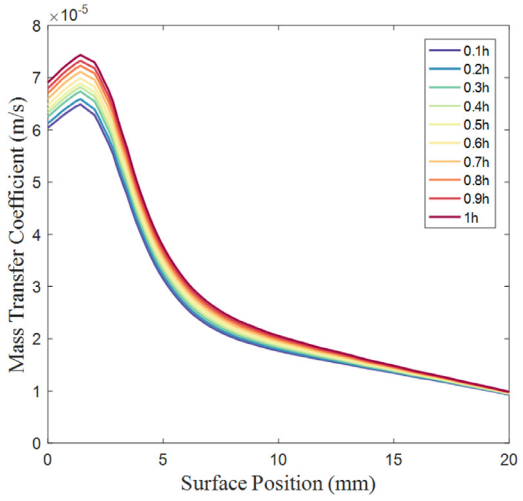

Fig. 7. The mass transfer coefficient distributions on silicon wafer at different time under ultrasound.

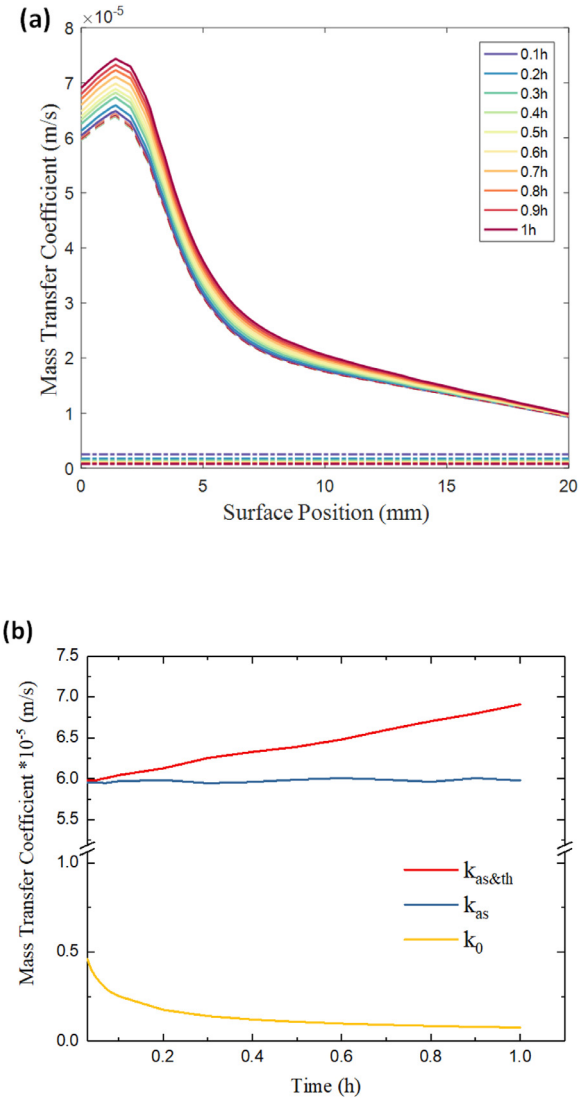

Fig. 8. (a) Mass transfer coefficients at different times under three simulated conditions: fluid-thermal coupling method (solid lines), calculation that ignored the thermal effect (dash lines), common reaction without ultrasound (dash dot lines). (b) Time-dependence of mass transfer coefficients in the center of wafer (surface position = 0) under the same conditions.

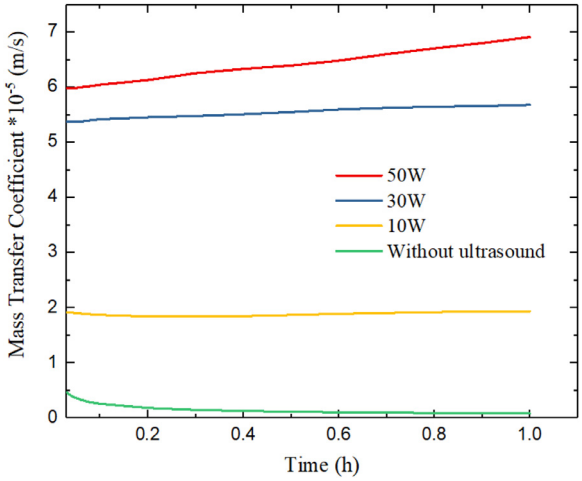

Fig. 9. Time-dependence of mass transfer coefficients in the center of wafer (surface position = 0) under ultrasound power of 10W, 30W, 50W and without ultrasound.

parison that the increase of mass transfer coefficient with time is due to the thermal effect of ultrasound. It's also worth noting that although the reaction rate at the interface increases by 2.4 times within an hour as shown in Fig. 6.b, the increase in mass transfer coefficient is not equally significant. Our further control simulations shows that the increase of diffusion coefficient and the decrease of solution viscosity are the main reasons for the increase of mass transfer coefficient, while the effect of reaction rate on mass transfer coefficient is not significant.

3.3.2. Effect of ultrasonic power

The mass transfer coefficients under different power of the ultrasound transducer is calculated and shown in Fig. 9. It is clear that the mass transfer coefficient is positively correlated with the ultrasound power, and the increase of the mass transfer coefficient with time is more significant under stronger ultrasound. According to the simulation results, as the ultrasound power increases, the flow rate of the solution increases and the temperature rises faster, thus leading to an enhancement of the mass transfer coefficient, which is exactly consistent with our previous discussion.

4. Conclusions

A novel computation model containing both acoustic streaming and ultrasonic thermal effect is established in this paper to quantitatively predict the mass transfer coefficient of liquid-solid reaction under ultrasound. Acoustic field calculation considering cavitation effect is applied to the computation model, and further carrying out the fluid-thermal coupling CFD simulation. The calculation results indicate that mass transfer coefficient under ultrasound is related to both time and space, which increases with the reaction time and has a maximum value near the center of the silicon wafer. When the ultrasonic power is 50W, the mass transfer coefficient is increased by more than one order of magnitude compared with the case without ultrasound. Mass transfer coefficient with ultrasound power of 10W and 30W is also calculated, which clearly shows that the mass transfer coefficient has a positive correlation with the ultrasonic power.

The effects of acoustic streaming and ultrasonic thermal effect on the mass transfer coefficient are separately studied by control simulation. It indicates that the enhancement of mass transfer coefficient by ultrasound is mainly attributed to acoustic streaming, while the thermal effect leads to the increase of the mass transfer coefficient with time by decreasing the viscosity and increasing the diffusion coefficient.

For further research, the effect of ultrasound frequency and the structure design of ultrasonic reactors can also be carried out by using the computation model in our paper. A more accurate model can further be established by using rigorous theory to replace several approximations in this manuscript.

Declaration of Competing Interest

The authors declare that they have no known competing financial interests or personal relationships that could have appeared to influence the work reported in this paper.

CRediT authorship contribution statement

Xingshuo Chen: Conceptualization, Methodology, Software, Writing – original draft. **Bayanheshig:** Supervision, Writing – review & editing. **Qingbin Jiao:** Conceptualization, Writing – review & editing, Resources. **Xin Tan:** Methodology, Resources. **Wei Wang:** Investigation, Visualization.

Acknowledgment

This work is supported by the National Natural Science Foundation of China (NSFC) (61227901, 61975199); Jilin Province Science & Technology Development Program in China (20190201304JC, 20190103158JH); Key core technology research project of the Chinese Academy of Sciences; Youth Innovation Promotion Association of the Chinese Academy of Sciences; and Dawn project of Changchun Institute of Optics, Fine mechanics and Physics.

References

[1] V.S. Moholkar, M.M.C.G. Warmoeskerken, Investigations in mass transfer enhancement in textiles with ultrasound, Chem. Eng. Sci. 59 (2004) 299–311.
[2] V.S. Moholkar, M.M.C.G. Warmoeskerken, Mechanism of mass transfer enhancement in textiles by ultrasound, AIChE J 50 (2004) 58–64.
[3] Y. Yao, W. Wang, K. Yang, Mechanism study on the enhancement of silica gel regeneration by power ultrasound with field synergy principle and mass diffusion theory, Int. J. Heat Mass Tran. 90 (2015) 769–780.
[4] L. Fu, L. Zhang, S. Wang, W. Cui, J. Peng, Synergistic extraction of gold from the refractory gold ore via ultrasound and chlorination-oxidation, Ultrason. Sonochem. 37 (2017) 471–477.
[5] Cass T. Miller, Michele M. Poirier-MeNeil, Alex S. Mayer, Dissolution of trapped nonaqueous phase liquids: mass transfer characteristics, Water Resour. Res. 26 (1990) 2783–2796.
[6] Susan E. Powers, Linda M. Abriola, Walter J.Weber Jr, An experimental investigation of nonaqueous phase liquid dissolution in saturated subsurface systems: steady state mass transfer rates, Water Resour. Res. 28 (1992) 2691–2705.
[7] Alex S. Mayer, Cass T. Miller, The influence of mass transfer characteristics and porous media heterogeneity on nonaqueous phase dissolution, Water Resour. Res. 32 (1996) 1551–1567.
[8] W. Dreybrodt, D. Buhmann, A mass transfer model for dissolution and precipitation of calcite from solutions in turbulent motion, Chem. Geol. 90 (1991) 107–122.
[9] I. Fujita, E. Hihara, Heat and mass transfer coefficients of falling-film absorption process, Int. J. Heat Mass Tran. 48 (2005) 2779–2786.
[10] L. Jiang, B. Wu, Y. Song, M. Yang, D. Wang, Y. Liu, Z. Xue, Mass transfer coefficient measurement during brine flush in a CO2-filled packed bed by X-ray CT scanning, Int. J. Heat Mass Tran. 115 (2017) 615–624.
[11] O. Dahlem, J. Reisse, V. Halloin, The radially vibrating horn: A scaling-up possibility for sonochemical reactions, Chem. Eng. Sci. 54 (1999) 2829–2838.
[12] S. Hyun, D.R. Lee, B.G. Loh, Investigation of convective heat transfer augmentation using acoustic streaming generated by ultrasonic vibrations, Int. J. Heat Mass Tran. 48 (2005) 703–718.
[13] Z. Xu, Keiji Yasuda, Shinobu Koda, Numerical simulation of liquid velocity distribution in a sonochemical reactor, Ultrason. Sonochem. 20 (2013) 452–459.
[14] B. Sajjadi, A.A.A. Raman, S. Ibrahim, Influence of ultrasound power on acoustic streaming and micro-bubbles formations in a low frequency sono-reactor: Mathematical and 3D computational simulation, Ultrason. Sonochem. 24 (2015) 193–203.
[15] S.I. Aanonsen, Barkve T, J.N. Tjøtta, S. Tjøtta, Distortion and harmonic generation in the nearfield of a finite amplitude sound beam, J. Acoust. Soc. Am. 75 (1984) 749–768.

[16] D.R. Bacon, E.L. Carstensen, Increased heating by diagnostic ultrasound due to nonlinear propagation, J. Acoust. Soc. Am. 88 (1990) 26–34.
[17] F.J. Trujillo, K. Knoerzer, A computational modeling approach of the jet-like acoustic streaming and heat generation induced by low frequency high power ultrasonic horn reactors, Ultrason. Sonochem. 18 (2011) 1263–1273.
[18] M.A. Margulis, Sonoluminescence and sonochemical reactions in cavitation fields. A review, Ultrasonics 23 (1985) 157–169.
[19] M.A. Margulis, Fundamental aspects of sonochemistry, Ultrasonics 30 (1992) 152–155.
[20] M.A. Margulis, Fundamental problems of sonochemistry and cavitation, Ultrason. Sonochem. 1 (1994) 87–90.
[21] Kenneth S. Suslick, David A. Hammerton, Raymond E. Cline, The sonochemical hot spot, J. Am. Chem. Soc. 108 (1986) 5641–5642.
[22] C. Ying, A.N. Yu, Distributions of the high temperature and the high pressure inside a single acoustically driven bubble, Sci. China Ser. A 45 (2002) 926–936.
[23] O. Louisnard, Nonlinear attenuation of sound waves by inertial cavitation bubbles, Phys. Procedia. 3 (2010) 735–742.
[24] O. Louisnard, A simple model of ultrasound propagation in a cavitating liquid. Part I: Theory, nonlinear attenuation and traveling wave generation, Ultrason. Sonochem. 19 (2012) 56–65.
[25] O. Louisnard, A simple model of ultrasound propagation in a cavitating liquid. Part II: Primary Bjerknes force and bubble structures, Ultrason. Sonochem. 19 (2012) 66–76.
[26] O. Louisnard, A viable method to predict acoustic streaming in presence of cavitation, Ultrason. Sonochem. 35 (2017) 518–524.
[27] R. Jamshidi, G. Brenner, Dissipation of ultrasonic wave propagation in bubbly liquids considering the effect of compressibility to the first order of acoustical Mach number, Ultrasonics 53 (2013) 842–848.
[28] F.J. Trujillo, A strict formulation of a nonlinear Helmholtz equation for the propagation of sound in bubbly liquids Part I: Theory and validation at low acoustic pressure amplitudes, Ultrason. Sonochem. 47 (2018) 75–98.
[29] F.J. Trujillo, A strict formulation of a nonlinear Helmholtz equation for the propagation of sound in bubbly liquids. Part II: Application to ultrasonic cavitation, Ultrason. Sonochem. 65 (2020) 105056.
[30] Q. Jiao, X. Tan, J. Zhu, Numerical simulation of ultrasonic enhancement on mass transfer in liquid–solid reaction by a new computational model, Ultrason. Sonochem. 21 (2014) 535–541.
[31] J.B. Keller, M. Miksis, Bubble oscillations of large amplitude, J. Acoust. Soc. Am. 68 (1980) 628–633.
[32] J.B. Keller, I.I. Kolodner, Damping of underwater explosion bubble oscillations, J. Appl. Phys. 27 (1956) 1152–1161.
[33] R. Toegel, B. Gompf, R. Pecha, D. Lohse, Does water vapor prevent upscaling sonoluminescence? Phys Rev. Lett. 85 (2000) 3165–3168.
[34] A.T. Preston, T. Colonius, C.E. Brennen, A reduced-order model of diffusive effects on the dynamics of bubbles, Phys. Fluids. 19 (2007) 502.
[35] Y. Zhang, Heat transfer across interfaces of oscillating gas bubbles in liquids under acoustic excitation, Int. Commun. Heat Mass Transf. 43 (2013) 1–7.
[36] R.E. Caflisch, M.J. Miksis, G.C. Papanicolaou, L. Ting, Effective equations for wave propagation in bubbly liquids, J. Fluid Mech. 153 (1985) 259–273.
[37] L. Bergamasco, D. Fuster, Oscillation regimes of gas/vapor bubbles, Int. J. Heat Mass Transf. 112 (2017) 72–80.
[38] Paul Mattaboni, Edward Schreiber, Method of pulse transmission measurements for determining sound velocities, J. Geophys. Res. 72 (1967) 5160–5163.
[39] J. Lighthill, Acoustic streaming, J. Sound Vib. 61 (1978) 391–418.
[40] K.R. Nightingale, G.E. Trahey, A finite element model for simulating acoustic streaming in cystic breast lesions with experimental validation, IEEE Trans. Ultrason. Ferr. 47 (2000) 201–215.
[41] Y. Guo, H. Xu, F. Guo, S. Zheng, Y. Zhang, Density and viscosity of aqueous solution of K2CrO4/KOH mixed electrolytes, Trans. Nonferrous. Met. Soc. China. 20 (2010) 32–36.
[42] D.L. Bideau, P. Mandin, M. Benbouzid, M. Kim, M. Sellier, Review of necessary thermophysical properties and their sensivities with temperature and electrolyte mass fractions for alkaline water electrolysis multiphysics modelling, Int. J. Hydrog. Energy. 44 (2019) 4553–4569.
[43] I.M. Hallaj, R.O. Cleveland, FDTD simulation of finite-amplitude pressure and temperature fields for biomedical ultrasound, J. Acoust. Soc. Am. 105 (1999) L7–L12.
[44] A.D. Pierce, in: “Acoustics, An Introduction to its Physical Principles and Applications”, Acoustical Society of America, New York, 1991, pp. 515–519.
[45] M.A. Margulis, I.M. Margulis, Calorimetric method for measurement of acoustic power absorbed in a volume of a liquid, Ultrason. Sonochem. 10 (2003) 343–345.
[46] J.-F. Dufreche, O. Bernard, P. Turq, Transport equations for concentrated electrolyte solutions: Reference frame, mutual diffusion, J. Chem. Phys. 118 (2002) 8116–8117.
[47] R.A. Robinson, R.H. Stokes, in: Electrolyte solutions, second ed., Butterworths Scientific Publications, 1970, p. 225.
[48] H. Seidel, L. Csepregi, A. Heuberger, H. Baumgartel, Anisotropic etching of crystalline silicon in alkaline solutions: I. Orientation dependence and behavior of passivation, J. Electrochem. Soc. 137 (1990) 3612–3626.
[49] Q. Jiao, X.Tan Bayanheshig, J. Zhu, J. Gao, The effects of ultrasound frequency and power on the activation energy in Si-KOH reaction system, Chin. Chem. Lett. 25 (2014) 617–620.
[50] James R. Welty, Charles E. Wicks, Robert E. Wilson, Gregory L. Rorrer, Fundamentals of Momentum, Heat and Mass Transfer, fifth ed., John Wiley & Sons, New York, 2000.